Check for updates

A ratiometric fluorescent sensor for detection of metformin based on terbium–1,10-phenanthroline–nitrogen-doped-graphene quantum dots†

Masoud Gazizadeh,[a] Gholamreza Dehghan[*a] and Jafar Soleymani [iD] [*b]

Metformin (MTF), an effective biguanide and oral antihyperglycemic agent, is utilized to control blood glucose levels in patients with type II diabetes mellitus, and the determination of its concentration in biological fluids is one of the main issues in pharmacology and medicine. In this work, highly luminescent nitrogen-doped graphene quantum dots (N-GQDs) were modified using terbium (Tb^{3+})–1,10-phenanthroline (Phen) nanoparticles (NPs) to develop a dual-emission ratiometric fluorescent sensor for the determination of MTF in biological samples. The synthesized N-GQDs/Tb–Phen NPs were characterized using different techniques to confirm their physicochemical properties. The N-GQDs/Tb–Phen NPs showed two characteristic emission peaks at 450 nm and 630 nm by exciting at 340 nm that belong to N-GQDs and Tb–Phen NPs, respectively. The results indicated that the emission intensity of both N-GQDs and Tb–Phen NPs enhanced upon interaction with MTF in a concentration-dependent manner. Also, a good linear correlation between the enhanced fluorescence intensity of the system and MTF concentration was observed in the range of 1.0 nM–7.0 μM and the limit of detection (LOD) value obtained was 0.76 nM. In addition, the prepared probe was successfully used for the estimation of MTF concentration in spiked human serum samples. In conclusion, the reported dual-emission ratiometric fluorescent sensor can be used as a sensitive and simple fluorimetric method for the detection of MTF in real samples.

1. Introduction

Diabetes mellitus, as a group of metabolic disorders, is determined by an increment in blood glucose level (hyperglycemia) due to a defect in insulin secretion, insulin action, or both. It has been reported that the number of diabetic patients will be increased to 642 million in the world by 2040.[1,2] The most common form of diabetes mellitus is type II or non-insulin-dependent diabetes, where the body becomes resistant to the effect of insulin.[3] It is one of the most important causes of mortality around the world. Different classes of antidiabetic agents including biguanides, sulfonylureas, thiazolidinedione, meglitinides, and alpha glucosidase inhibitors have been developed for administration to diabetic patients.[3–5]

Metformin hydrochloride (MTF; Fig. 1) is an effective biguanide and oral antihyperglycemic agent, which is widely

used to control blood glucose level (as the first-line treatment) in patients with type II diabetes mellitus. An increase in the incidences of lactic acidosis results in a high concentration of MTF in plasma.[6,7] So, the determination of its concentration in biological fluids is one of the main issues in pharmacology and medicine.

Diarrhea, nausea, gas, heartache, and heartburn are the most important side effects of MTF. Of course, these are mild effects and will disappear in a short time, but in some cases, the mentioned cases may worsen. Body tremors, nervous disorders, high heart rate, excessive sweating, drowsiness, and acidosis confusion are some other side effects of the MTF overdose.[7]

A literature survey showed that different analytical methods such as high-performance liquid chromatography (HPLC),[8,9] liquid chromatography-mass spectrometry (LC-MS),[10] spectrophotometry,[5,11] spectrofluorimetry,[5,12,13] gas chromatography-mass spectrometry (GC-MS),[14] capillary electrophoresis (CE),[15] potentiometry,[11] HPLC-UV,[16,17] and HPLC-MS[18,19] have been reported for quantitative measurement of MTF in human plasma, urine and tablet formulations (Table 1). Despite the effectiveness, most of these methods suffer from some drawbacks such as high cost, time-consuming and hard experimentation

[a]*Department of Animal Biology, Faculty of Natural Sciences, University of Tabriz, Tabriz, Iran. E-mail: gdehghan@tabrizu.ac.ir; Tel: +98 41 3339 2739*

[b]*Pharmaceutical Analysis Research Center, Tabriz University of Medical Sciences, Tabriz, Iran. E-mail: jsoleymanii@gmail.com; soleymanij@tbzmed.ac.ir; Tel: +98 41 3337 5365*
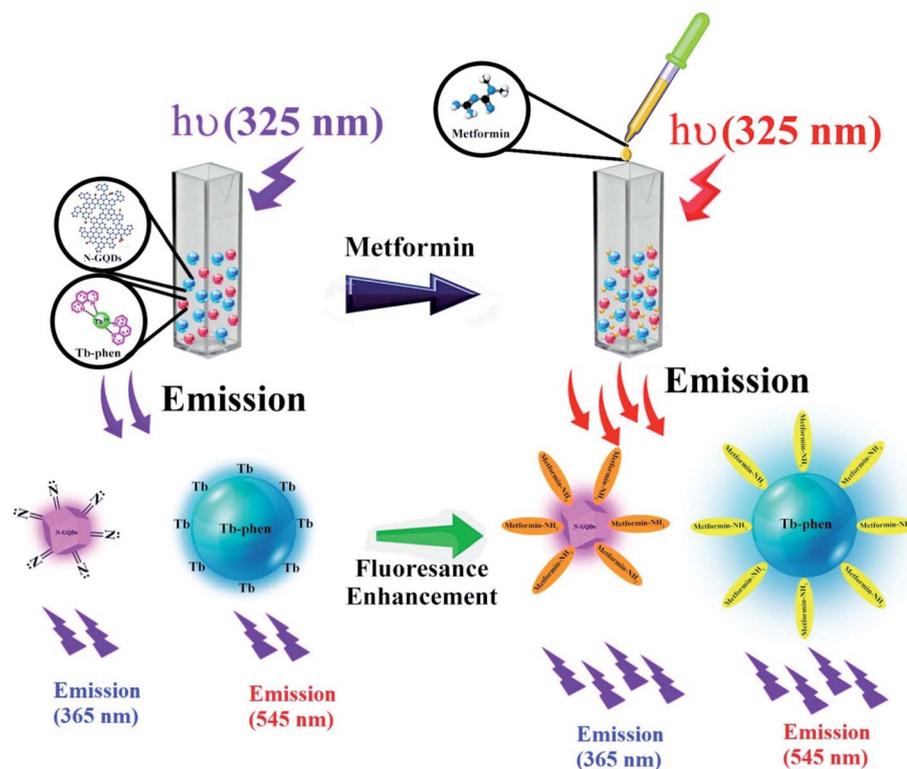
Scheme 1 Design for the determination of MTF based on its enhancing effect on the fluorescence emission of N-GQDs and Tb–Phen NPs.
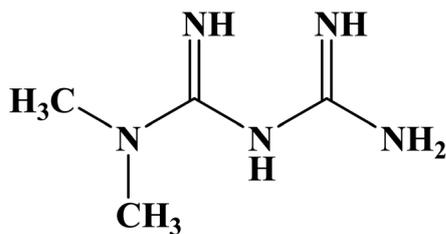

Fig. 1 Chemical structure of MTF.

processes, and need for damaging chemical reagents, *etc.*[5] To overcome these disadvantages, many researchers are trying to develop new sensitive, simple, selective, and inexpensive methods for the determination of different drugs such as MTF in biological samples.

Carbon-based materials have significant applications in different areas including chemistry, biomedical, materials, and some other fields because of their environmental friendliness.[20,21] Carbon dots (CDs), as a subgroup of quantum dots (QDs), are nanomaterials with dimensions smaller than 10 nm.[22,23] These materials have gained considerable attention due to their unique properties including bright photoluminescence, chemiluminescence, high quantum yield (QY), photoinduced electron transfer, low toxicity, small size, good biocompatibility, and numerous low-cost supplies.[20,22,24] Doping and modifying these materials with some molecules can change

Table 1 Comparison between the proposed method and some other reported methods for the detection of MTF

Method	Linear range ($\mu g\ mL^{-1}$)	LOD ($\mu g\ mL^{-1}$)	Ref.
HPLC	0.015–0.05	0.015	8
RP-HPLC	125–750	1.88	9
HPLC-MS-MS	0.01–10	0.00098	18
GC-MS	0.1–3.0	0.040	13
Capillary zone electrophoresis	50–500	2.11	14
Electrochemical method (GNF-PMB/SnO$_2$/F on transparent glass electrodes)	12.92–129.2	1.29	49
Voltametric method	0.129–516.7	0.065	50
HPLC-UV	0.125–2.5	0.062	51
LC-MS/MS	0.05–5	—	52
Spectrofluorimetry (BSA-GNCs as a fluorescent probe)	0.028–1.42	0.009	53
Spectrofluorimetry (Tb–Phenphen-AgNPs as a fluorescent probe)	0.097–0.48	0.055	54
N-GQDs/Tb–Phen NPs	0.387–904.2	0.0038	This work

their optical and electronic characters and provide some unique properties.

As a class of zero-dimensional materials, graphene quantum dots (GQDs) consist of single or multi-layers of graphene sheets with lateral dimensions less than 100 nm in size.[24,25] These materials possess some unique properties including large surface/volume ratio, small size, good aqueous solubility, biocompatibility, low toxicity, electronic and optical properties,[26–28] which have gained the immense interest of the scientific community with widely used in various fields such as bioimaging, chemical-sensing, bio-sensing, drug delivery, photocatalysis, optoelectronic devices, etc.[29–31] Also, these materials have been widely used as fluorescent, high sensitive, and simple probes for the determination of metal ions, cancer cell detection, cellular interaction, and some other biological applications.[32,33]

Recently, the fluorescent probes that employed sensitized luminescence of rare earth complexes are widely used in various analytical fields, especially in scientific research in analytical chemistry, biomedicine, and biology due to their high sensitivity.[34,35] So, in the present study, high luminescent nitrogen-doped GQDs (N-GQDs) was modified by using terbium (Tb^{3+}; lanthanide ions)–1,10-phenanthroline (Phen) nanoparticles (N-GQDs/Tb^{3+}–Phen NPs) and used as highly sensitive and dual-emission ratiometric fluorescent nanosensor for the selective detection of MTF in real plasma samples in which the ratio of fluorescence intensity at two different emission wavelengths under one excitation wavelength is measured. High sensitivity and intrinsic reliability are two of its benefits, which reflect the self-calibration provided by monitoring two (or more) emissions. Also, this technique provides a visualization capability with naked eyes under UV lamp when operating the measurements.[36] We chose lanthanide ions due to their inexpensive cost, great internal quantum efficiencies, and intense luminescence properties and Phen because of its enhancing effect on the luminescence of Tb^{3+}. The prepared nanocomposite was characterized using different methods including scanning electron microscope (SEM), TEM (transmission electron microscopy), Fourier-transform infrared spectroscopy (FTIR), and UV-vis absorption spectroscopy and used for the fluorimetric detection of MTF.

2. Experimental

2.1. Chemicals

Phen was purchased from Fluka (Buchs, Switzerland). Citric acid, ethylenediamine, disodium hydrogen phosphate (Na$_2$HPO$_4$), sodium dihydrogen phosphate (NaH$_2$PO$_4$), sodium acetate, acetic acid, cetyltrimethylammonium bromide (CTAB), and dimethylsulfoxide (DMSO) were provided from Merck Company (Darmstadt, Germany). Terbium(III) chloride hexahydrate (TbCl$_3$; Across), ethanol, methanol, acetone, propanol, acetonitrile, chloroform, sodium dodecyl sulfate (SDS), aerosol-OT or sodium bis(2-ethylhexyl) (AOT), Brij, Triton X-100, and Tween 20 were obtained from Sigma-Aldrich (St. Louis, MO, USA). MTF was purchased from Osveh Pharmaceutical Company (Tehran, Iran). All reagents were of analytical grade.

A 0.05 M acetate buffer solution was prepared by dissolving 1.93 g of sodium acetate (47.1 mM) and 0.088 g of acetic acid (2.9 mM) in 500 mL distilled water. Then, the pH level of the prepared buffer solution was adjusted using HCl and NaOH.

2.2. Instrumentation

The morphology of N-GQDs, Tb–Phen, and N-GQDs/Tb–Phen NPs was characterized by using FESEM on FEG-SEM MIRA3 TESCAN (Brno, Czech Republic). FTIR (Shimadzu model FTIR prestige 21, Tokyo, Japan) and attenuated total reflection Fourier-transform infrared (ATR-FTIR; a BRUKER, Tensor 27) spectroscopies were carried out for the investigation of the functional groups of N-GQDs and N-GQDs/Tb–Phen NPs, respectively (in the range between 400–4000 cm^{-1}). Also, the dynamic light scattering (DLS) and zeta potential (ZP) techniques were applied to the analysis particles' size, size distribution, and the stability of synthesized nanomaterials at room temperature on Zetasizer Nano ZS90, Malvern Instruments (Malvern, UK). UV-Vis absorption spectra of the samples were recorded on a T60, PG Instruments LTD. (Leicestershire, UK) spectrophotometer, and all fluorescence spectra of the samples were measured using a Jasco FP-750 spectrofluorimeter (Kyoto, Japan).

2.3. Synthesis of N-GQDs

N-GQDs were produced using a previously described solvothermal approach.[19,37] Briefly, about 1.0 g citric acid and 400 μL of ethylenediamine were mixed in 15 mL distilled water. The prepared mixture was stirred for 1 min to mix well. Then, the synthesized solution was transferred into a 20 mL Teflon lined stainless hydrothermal synthesis autoclave and heated up to 180 °C in an oven and kept for 8 h. The prepared solution was centrifuged for 15 min at 10 000 rpm for the removal of any insoluble substances.

2.4. Preparation of Tb–Phen NPs

A previously reported method was utilized for the preparation of Tb–Phen NPs.[38,39] Briefly, 2.5 mL of Phen solution (in ethanol, 100 mM) was added into 5 mL of TbCl$_3$ solution (in distilled water, 100 mM) and stirred vigorously for 20 min. The produced solution was then heated up to 160 °C and remained for 2 hours after cooling at room temperature, the mixture was centrifuged for 10 min at 13 000 rpm. Finally, a dialysis bag (1 kDa) was used for the elimination of unreacted reactants. For this purpose, prepared precipitates were dispersed into a dialysis bag, which was then kept in a beaker containing deionized water and absolute ethanol for 8 h. After suitable dilutions, the prepared samples were used for further analysis.

2.5. Fluorimetric assay of MTF by N-GQDs/Tb–Phen NPs

Determination of MTF was performed by monitoring the fluorescence intensity of N-GQDs/Tb–Phen NPs. For this purpose, a fixed concentration of N-GQDs/Tb–Phen NPs was incubated for 10 min with various concentrations of MTF from 3.0 nM to 3.0 μM in 500 μL acetate buffer solution (0.05 M, pH 7.5). Then,

the fluorescence spectra of the samples were measured at 365 nm ($\lambda_{em(N-GQDs)}$ = 365 nm) and 545 nm ($\lambda_{em(Tb-Phen)}$ = 545 nm) by exciting at 325 nm (Scheme 1).

2.6. Selectivity of N-GQDS/Tb–Phen NPs for MTF

The selectivity of the proposed method for the detection of MTF was investigated by testing the effect of some species present in the real samples on the emission intensity of N-GQDs/Tb–Phen NPs. For this purpose, 120 μL of interfering substance stock solutions (0.03 to 3 μM) including cations (Na^+, K^+, Mg^+, Cu^+, Pb^+, and Zn^+), some drugs (naproxen, mesalazine, amlodipine, cephalexin, acetaminophen, amoxicillin, aspirin, diclofenac, and cetirizine) and vitamins (B1, B2, and C) were added to 40 and 500 ppm of N-GQDs/Tb–Phen NPs suspension containing 3 nM MTF. Then, the final volume of the prepared solutions was reached 4.0 mL by using distilled water. Finally, the fluorescence intensity of the solutions was observed at 365 nm and 545 nm by exciting at 325 nm.

2.7. Fluorimetric detection of MTF in real samples

Detection of MTF was also performed in plasma samples (as a real media) by using the proposed method. For this purpose, healthy human plasma was provided by the Iranian Blood Transfusion Organization (IBTO). Before further analysis, various concentrations of MTF were spiked in serum samples and deproteinized by using the following procedure: 1.5 mL of acetonitrile was added to the previously spiked samples and mixed well for 2 min. Then, the prepared mixtures were centrifuged at 13 000 rpm for 15 min. Finally, the supernatants were used for further analysis.[34,40]

3. Results and discussion

3.1. Characterization studies

The morphology and size of synthesized nanoparticles were investigated using SEM and TEM analysis. Fig. 2 shows the TEM images of N-GQDs (B) and Tb–Phen NPs (A). Also, Digi-miser software was used to measure particle's diameter. For this purpose, 100 separate nanoparticles were measured with software and a histogram was drawn based on the obtained data. This diagram shows the frequency of nanoparticles in a certain diameter range and thus shows a report of statistical parameters such as average, minimum, maximum, *etc.* of nanoparticle size. On the other hand, the actual size of the N-GQDs (Fig. 2B), Tb–Phen NPs (Fig. 2A), and N-GQDs/Tb–Phen NPs (Fig. 2B) the average particle sizes of the N-GQDs, Tb–Phen NPs, and N-GQDs/Tb–Phen NPs are estimated to be 2.36, 3.74 and 80 nm, respectively.

In addition, FTIR spectroscopy was used to investigate the functional groups of N-GQDs, Tb–Phen NPs, and N-GQDs/Tb–Phen NPs. In the FTIR spectrum of N-GQDs, the characteristic peaks at 3245, 1638, 1076, and 1577 cm^{-1} were observed, which are related to the O–H, –NH$_2$, C–C, and C=O stretching-vibration peaks, respectively (Fig. 2C). The existence and accessibility of the OH, NH$_2$, and COOH functional groups in the surface of the resultant NPs were confirmed by these

findings.[20] Also, Fig. 2C shows the ATR-FTIR spectra of Tb–Phen NPs, N-GQDs/Tb–Phen NPs, and N-GQDs/Tb–Phen NPs. As can be seen, the characteristic vibrational absorption peaks were observed at 1545 cm^{-1} and 1424 cm^{-1}, which were related to the COO$^-$ functional group of carboxylate in the rare earth complexes.[41,42] The results confirmed the coordination of the rare earth ions with the oxygen atoms of carbonyl groups. On the other hand, the characteristic peaks of Phen showed a slight shift from 853 cm^{-1} to 847 cm^{-1} (related to C–H bonds) and from 1586 cm^{-1} to 1590 cm^{-1} (related to C=N bonds). This is due to the coordination of rare-earth ions with Phen molecule.[41,42] According to this figure, it can be concluded that the general shape of the N-GQDs/Tb–Phen NPs is a mixed form of Tb–Phen NPs and N-GQDs, confirming the synthesis of N-GQDs/Tb–Phen NPs. Also, the ATR-FTIR spectrum of N-GQDs/Tb–Phen NPs in the presence of MTF is shown in Fig. 2C. As shown in the figure, the observed alterations in the intensities of bands and the shifts in the band positions confirm the interaction of MTF with N-GQDs/Tb–Phen NPs.

On the other hand, the stability and the surface charge of prepared Tb–Phen NPs were determined using zeta analysis. In general, particles with zeta values greater than +30 mV or less than −30 mV are considered to have sufficient repulsive force to gain high degrees of stability.[20,43] The obtained results showed more negative zeta potential values for N-GQDs/Tb–Phen NPs and the stability of N-GQDs/Tb–Phen NPs can be influenced by their negative charge (Fig. 1S†). N-GQDs and N-GQDs/Tb–Phen NPs were also subjected to DLS analysis, with the findings revealing an increase in the particle size of N-GQDs/Tb–Phen NPs (Fig. 1S†).

3.2 Spectroscopic properties of the nanoparticles

The formation of N-GQDs/Tb–Phen NPs was evaluated by recording the absorption spectra of N-GQDs, Tb–Phen NPs, and N-GQDs/Tb–Phen NPs. As shown in Fig. 2D, the absorption spectrum of N-GQDs/Tb–Phen NPs in the absence of MTF shows two characteristic peaks at 266 nm and 348 nm, which were mainly from the absorption of Tb–Phen NPs and N-GQDs, respectively. Also, the observed absorption peak at 266 nm confirms the formation of Tb–Phen NPs and energy transfer from Phen to Tb^{3+}.[38,44] On the other hand, the absorption spectrum of N-GQDs/Tb–Phen NPs was recorded in the presence of 1.0 μM MTF, and the results showed the enhancing effect of MTF on the UV absorption of N-GQDs/Tb–Phen NPs (Fig. 2D), demonstrating that MTF increases the absorption of N-GQDs and Phen within N-GQDs/Tb–Phen NPs and energy transfer to Tb^{3+}.[38] The UV absorption of MTF showed no significant overlap with the absorption spectrum of N-GQDs/Tb–Phen NPs.

3.3. Calculation of the QY of Tb–Phen NPs

The QY of Tb–Phen NPs was investigated in aqueous media spectrophotometrically using a comparative method at an excitation wavelength of Tb–Phen NPs.[45] L-Tyrosine (QY 14% in water) was regarded as the reference material. To determine, the concentration of Tb–Phen NPs and the L-tyrosine solutions were
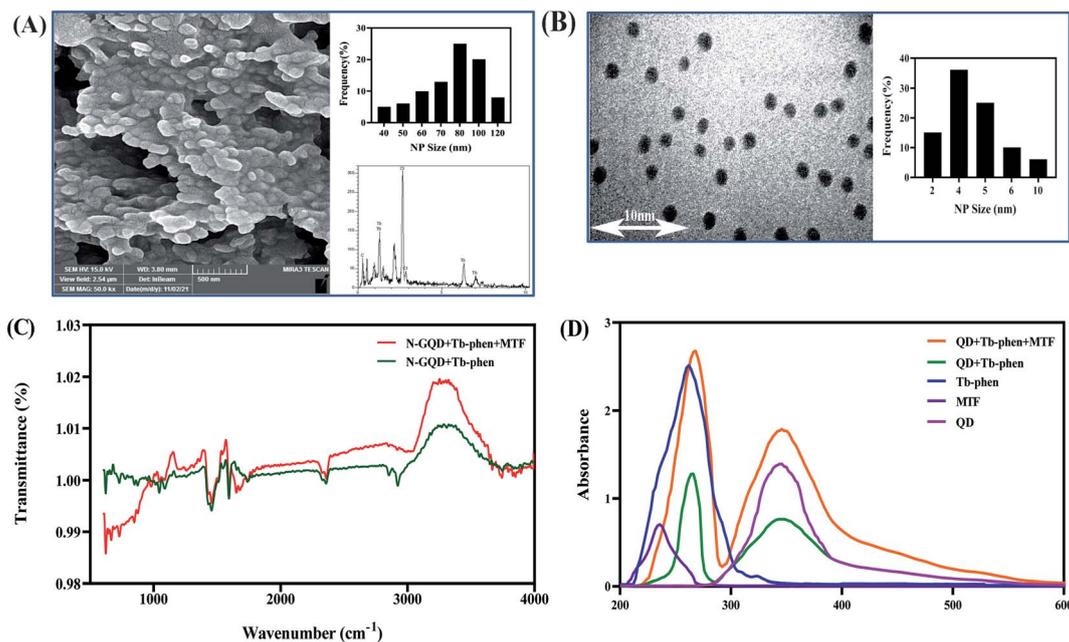
Fig. 2 (A) FESEM images and EDX of Tb–Phen NPs, (B) TEM image of N-GQDs, (C) ATR-FTIR spectrum of N-GQDs/Tb–Phen NPs with and without MTF and (D) absorption spectra of N-GQDs/Tb–Phen NPs (in the absence of MTF), Tb–Phen, N-GQDs, Tb–Phen NPs with MTF.

adjusted to measure absorbances below 0.1. After then, the fluorescence emission of them were recorded at least three concentrations and plotted a calibration curve to obtain slope for calculation of QY using the following equation.

$$Q_S = Q_R \text{ (slope of NPs)/(slope of ref)} \left(\frac{\eta_S}{\eta_R}\right)^2$$

in which "S" and "R" denote Tb–Phen NPs and L-tyrosine, respectively. QYs of TbNPs and L-tyrosine are Q_S and Q_F, respectively. η denotes the refractive index which is equal to one for aqueous solutions.

The final QY was calculated as the area of the emission spectra from 400 nm to 600 nm. The QY of fluorescence for the Tb–Phen NPs was estimated to be 31.6%. The high fluorescence QY of Tb–Phen NPs could be related to the smaller size of Tb–Phen NPs. It has been reported that the higher levels of doped nitrogen resulted in increased photoluminescence, confirming the findings of this research.[46]

3.4. Optimization of experimental conditions

To obtain a maximum sensitivity of the prepared system toward MTF, the effect of some factors affecting the response of the system including pH values, time, temperature, the types and volume of solvent, surfactant, buffer, and concentrations of buffer solution was studied and optimum conditions were selected. The fluorescence ratio changes (F_{545}/F_{365}) were used as an analytical response for this purpose. All the experiments were carried out in the presence of 1.0 μM of analyte (MTF). To check the stability of the produced probe, the effect of ultraviolet (UV) light, and salt was also investigated.

The three different types of buffer solution including phosphate, Tris–HCl, and acetate buffers were assessed. As

mentioned above, the prepared N-GQDs/Tb–Phen system exhibited two characteristic emission bands at 365 nm and 545 nm by exciting at 325 nm. The results showed that the maximum fluorescence ratio (F_{545}/F_{365}) of the system was achieved by the use of acetate buffer solution (Fig. 2S†). As obvious, acetate has a carboxylic acid and Tris–HCl has an amine and three alcohol functional groups. While phosphate has oxygen anions which extremely reactive towards Tb^{3+} vacant orbitals. As a mechanism, there is a dynamic competition between MTF and 1,10-phenanthroline to attach to the Tb ions, resulting in enhancing the fluorescence intensity of the nanoprobe. Upon addition of the buffer to the media, there is competition among buffer, MTF, and 1,10-phenanthroline. However, the interaction between phosphate and Tb^{3+} is strengths as which resulted in the quenching of the nanoprobe by replacing 1,10-phenanthroline molecules with phosphate ions. Regarding the acetate and Tris–HCl functional groups, the acetate buffer can more effectively compete with the 1,10-phenanthroline molecules because of low steric and conformational hindrance. So, this type of buffer was used for further studies. Then, the effect of various concentrations of acetate buffer solution (10, 20, 50, 100, and 200 mM) on the system signal and fluorescence ratio was evaluated and the obtained results are shown in Fig. 2S.† According to this figure, the maximum emission ratio of the prepared system was observed at 50 mM acetate buffer solution and used for further analysis. The OH groups of water molecules can cover the terbium ions at lower concentrations of buffer and quench the emission intensity of the system due to OH oscillation. However, with increasing the concentration of buffer, acetate ligands can probably prevent Tb^{3+} ions from coordinating water, so, the emission intensity is increased.[47]

In addition, the effect of pH was investigated using buffers with different pH values ranging from 2.5 to 11.5. As shown in Fig. 3A, the fluorescence ratio of the system was strongly dependent on pH and the maximum signal was achieved at pH 7.5. In acidic and basic conditions, the emission intensity of Tb–Phen NPs was quenched. However, the emission of N-GQDs NPs was fixed and slightly increased. So, pH 7.5 was selected for further studies.

On the other hand, the effect of time (0–40 min) on the fluorescence intensity was investigated. As shown in Fig. 3S,† no change of fluorescence ratio and the signal of the system was observed and the emission ratio was stable during the time even after 4 h. As a result, the prepared system's response was unaffected by the progressing of time.

The effect of temperature ranging from 0 to 45 °C on the emission intensity of the prepared N-GQDs/Tb–Phen NPs was evaluated under the optimum conditions and the obtained results showed that the fluorescence ratio was gradually increased with increasing temperature up to 20 °C and then decreased (Fig. 3S†). So, 20 °C was selected as an optimum temperature for further experiments.

Furthermore, the concentration ratio of N-GQDs NPs to Tb–Phen NPs for the preparation of N-GQDs/Tb–Phen NPs was assessed by using a fixed concentration of N-GQDs (40 ppm) and variable concentrations of Tb–Phen NPs (ranging from 100 ppm to 1500 ppm). The obtained results indicated that the maximum fluorescence intensity ratio was achieved when the concentration of Tb–Phen NPs was 500 ppm (Fig. 3S†).

Effect on the polarity of the media *i.e.* solvent type is one of the important factors affecting the fluorescence emission which is recommended by the guidelines. The effect of different solvents including water, methanol, ethanol, propanol, acetone, chloroform, and acetonitrile on the fluorescence signal of the prepared system was tested. The obtained results indicated that the maximum signal of the emission ratio was achieved in the presence of acetone (as a solvent) (Fig. 3B). Also, the effect of solvent (acetone) concentration (from 0.05 mL to 2 mL) on the fluorescence ratio of the system was investigated. According to the data given in Fig. 3C, the fluorescence ratio of the N-GQDs/Tb–Phen NPs was maximum when the acetone concentration was 0.75 mL. So, the concentration of acetone was chosen to be 0.75 mL for further studies.

The effect of different surfactants such as CTAB, SDS, AOT, X100, Tween 20, and Brij on the emission ratio was also studied. The critical micelle concentration (CMC) is the lowest concentration of a surfactant at which micelles can form.[48] The results of the present study indicated that at concentrations of CMC and in the absence and presence of MTF, compatible enhancement of fluorescence ratio was observed in the presence of SDS (Fig. 4S†) (A). However, at concentrations lower CMC, the fluorescence ratio enhanced using AOT and CTAB with and without MTF, respectively (Fig. 4S†) (B).

3.5. Analytical features of the developed method

The detection ability of the system towards MTF was investigated. For detecting MTF, N-GQDs/Tb–Phen NPs were dispersed in acetate buffer solution and excited at 325 nm. The emission spectrum of N-GQDs/Tb–Phen NPs showed two characteristic peaks at 545 nm and 365 nm, which were related to Tb–Phen NPs and N-GQDs, respectively. The observed emission peak of Tb–Phen NPs arises from $^5D_4 \rightarrow ^7F_J$. Also, the emission peak of Tb–Phen NPs at 545 nm was much stronger than the same

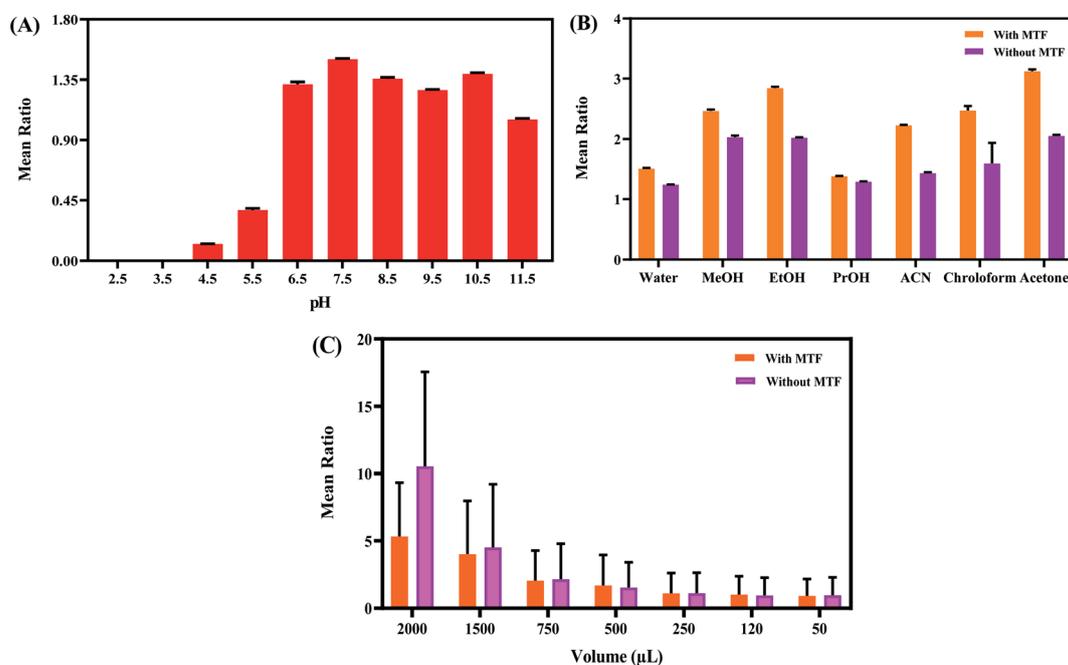**Fig. 3** (A) The effects of pH, (B) the effects of different solvents on the response of the N-GQDs/Tb–Phen NPs sensor in the presence of 1.0×10^{-6} M MTF, (C) optimation volume of solvent with in the presence of 1.0×10^{-6} M MTF.

amount of Tb^{3+} ions alone. This is due to the antenna effect and intramolecular energy transfer process from Phen to Tb^{3+} ions.[38] Also, the observed emission intensity of N-GQDs at 365 nm is due to the blocking of non-radiative electron recombination and creating more radiative centers by the elimination of local trap positions on the surface of N-GQDs.[49] The results showed a concentration-dependent MTF detecting procedure. As demonstrated in Fig. 4A, upon addition of concentrations of MTF (ranging from 1.0 nM to 7.0 μM) into the solution mixture containing 1.0 mL acetate buffer (pH 7.5), Tb–Phen NPs (500 ppm), and N-GQDs (40 ppm), the characteristic fluorescence peaks of N-GQDs and Tb–Phen NPs were increased in a concentration-dependent manner. Also, the relationship between MTF concentration in standard solution and fluorescence intensity of the prepared system was studied.

To investigate the applicability of the proposed dual-emission ratiometric fluorescent sensor, determination of MTF was performed under the optimum conditions in the human serum samples based on the described procedure. The obtained results indicated that by increasing MTF concentration the fluorescence intensity was increased, which was proportional to the MTF concentration. Also, a linear correlation was observed between the fluorescence ratio (F_{545}/F_{365}) concentration of MTF in the range of 1.0 nM to 7.0 μM with

a good $R^2 = 0.9997$ ($F_{545}/F_{365} = 8 \times 10^6 C + 0.5458$). Also, LOD and LOQ values were found to be 0.76 nM and 2.5 nM, respectively (Fig. 4B). The developed method provides better LOD than about all of the reported methods in Table 1. As can be seen, our method showed comparable or a better detection limit than the previously reported methods. Most of the reported methods require time-consuming/complicated sample pretreatment and professional operators, which limits the application of these approaches for on-site and real-time determination of MTF. However, the developed method is inexpensive, rapid, precise and sensitive for screening of MTF.

3.6. Recovery and accuracy

Also, the added-found procedure was used to investigate the intraday and inter-day assay accuracy and precision of the system for the determination of MTF.[50] For this purpose, three different concentrations of MTF were spiked into the serum samples and intraday and inter-day precision and accuracy were determined by injecting three different concentrations at three different times of the same day and these same concentrations on three different days. The obtained results are given in Table 2. As can be seen, the percentage absolute recovery of MTF from plasma showed satisfactory precision and accuracy. Therefore, the findings showed satisfactory precision, accuracy, and recovery with high sensitivity and selectivity for the detection of MTF in real samples without needing a separation technique in analysis.

3.7. Stability study

The stability of the proposed method in plasma samples was assessed by analyzing the samples at different concentrations of N-GQDs and Tb–Phen NPs during the sample and storage procedure. After 0 to 12 hours of exposure to room temperature, the plasma samples were tested for short-term stability. Also, the free/thaw stability was determined after one freeze/thaw cycle at −20 °C. All stability studies yielded quantities that were compared to freshly prepared samples. The precision for freeze/thaw samples ranged from 0.63–8.18%, confirmed that the proposed system was stable in plasma for three cycles when stored at −20 °C. Also, short-term temperature showed satisfactory precision. These results indicated the stability of the developed system under the experimental conditions of the analytical runs (Table 3).
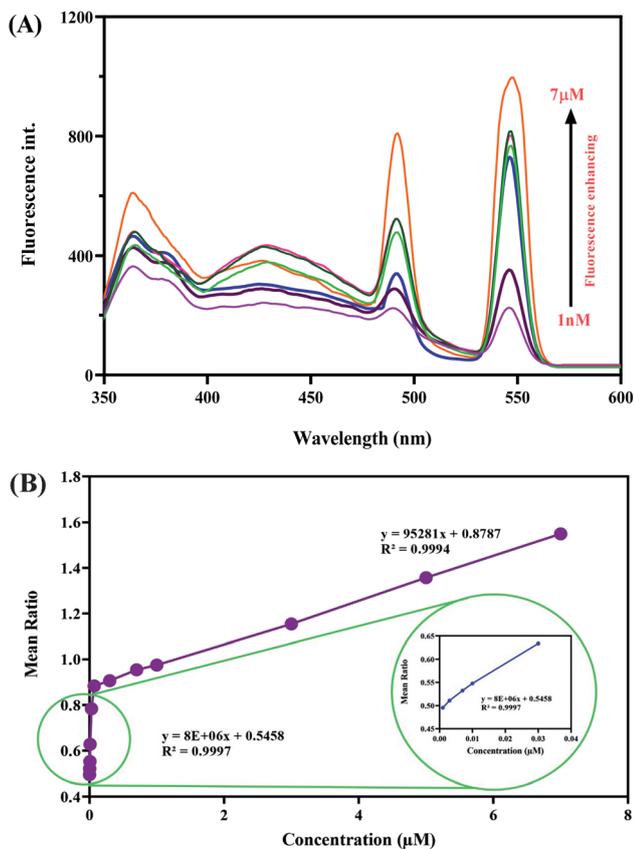
Fig. 4 (A) The emission intensity of N-GQDs/Tb–Phen NPs in the presence of additional concentrations of MTF and (B) the linear relationship between the fluorescence ratio of N-GQDs/Tb–Phen NPs of MTF concentration under the optimum concentrations.

Table 2 Precision, accuracy, and recoveries for the determination of MFT in plasma media

Sample	Concentration (M)	(RSD%)	Accuracy (RE%)	Recovery (%)
Intra-day	1.0×10^{-8}	2.5	3.0	103.0
	7.0×10^{-7}	0.7	12.8	112.8
	7.0×10^{-6}	1.5	0.5	100.5
Inter-day	3.0×10^{-8}	2.1	−4.1	95.8
	1.0×10^{-6}	2.4	17.1	117.1
	7.0×10^{-6}	2.0	3.2	103.2

Also, the effect of UV light on the response of the system was investigated for 360 min. The results indicated that the emission intensity was stable up to 120 min and then, a significant decrease was observed in the maximum emission intensity of Tb–Phen NPs (about 200 units) and N-GQDs (about 35 units). The fluorescence ratio changes of the system in the presence of UV light was shown in Fig. 5S.† However, the quenching effect of UV light on the fluorescence intensity of Tb–Phen NPs was greater than N-GQDs.

Since most of the biological or chemical samples typically exist in buffer solutions containing sodium or potassium, the salt effect on the response of the system was investigated using different concentrations of NaCl salt (5, 25, 50, 100, and 250 mM). As demonstrated in Fig. 5S,† the emission intensity of both Tb–Phen NPs and N-GQDs decreases with enhancing the concentration of salt.

Also, the stability of the prepared nanoparticles (N-QGDs and Tb–Phen NPs) was investigated during 28 days and the results showed no significant changes in the fluorescence intensity ratio and stability of the prepared nanoparticles.

3.8. Study of interferences

Based on the Food and Drug Administration guidelines (FDA), to investigate the selectivity of the prepared nanosensor, the possible effect of some coexisting interfering species in the real samples on the response of the developed nanoprobe was assessed under the optimized conditions in the presence of 3.0 nM of MTF.[50] In this work, the effects of ions such as Na^+/K^+ (main role in cell membrane function in the charge balance between the two sides of the membrane as a sodium/potassium pump, etc.), Mg^{2+} (role in ATP activation and stability of polyphosphate compounds in DNA and RNA synthesis), Zn^{2+} (role in wound healing, immune system function and activation of some enzymes, etc.), Ca^{2+} (role in bone strength and blood pressure regulation, etc.), Cl^- (in the nervous system, the function of glycine and GABA is related to the level of chlorine ions in specific neurons. In addition, chlorine ion plays a role in maintaining the acid–base balance of the blood, which is responsible for regulating its level by the kidneys), Cu^{2+} (main inscription to the production of respiratory enzyme cytochrome oxidase C and superoxide dismutase, etc.), some co-prescribed pharmaceutical drugs that can be prescribed and used simultaneously with MTF, other metabolites and amino acids were checked. The names of the agents and obtained results of their effects on the system are presented in Table 4. According to the data obtained the tolerance limits (the concentration ratio of

Table 4 Effects of some common interfering substances on the detection of MTF (3 nM) under the optimum conditions

Interfering agent	The concentration of interfering agent (M)	Ratio	RSD (%)
Na^+	3.0×10^{-6}	1000	2.4
K^+	3.0×10^{-6}	1000	2.4
Mg^{2+}	3.0×10^{-6}	1000	2.4
Zn^{2+}	3.0×10^{-6}	1000	2.4
Ca^{2+}	3.0×10^{-6}	1000	3.6
Cl^-	3.0×10^{-6}	1000	−7.8
Cu^{2+}	3.0×10^{-8}	10	5.1
Cd^{2+}	4.5×10^{-7}	150	2.7
Pb^{2+}	9.0×10^{-7}	300	−7.1
Starch	3.0×10^{-6}	1000	3.6
Lactose	3.0×10^{-6}	1000	2.3
Uric acid	3.0×10^{-7}	100	4.9
Sucrose	3.0×10^{-6}	1000	2.3
Vitamin B1	1.5×10^{-6}	500	2.3
Vitamin B2	3.0×10^{-7}	100	−7.5
Vitamin C	3.0×10^{-6}	1000	3.4
Naproxen	2.1×10^{-6}	700	2.4
Mesalazine	2.4×10^{-6}	800	5.1
Amlodipine	3.0×10^{-6}	1000	2.7
Cephalexin	2.4×10^{-6}	800	2.4
Amoxicillin	2.4×10^{-6}	800	−7.3
Diclofenac	2.4×10^{-6}	800	3.6
Cetirizine	3.0×10^{-6}	1000	5.5
Acetaminophen	3.0×10^{-6}	1000	1.9
Aspirin	1.5×10^{-6}	500	−7.8
Penicillin	2.1×10^{-6}	700	5.6
Erythromycin	3.0×10^{-6}	1000	1.9
Ceftriaxime	3.0×10^{-6}	1000	−0.1

interfering species or analyte that produces a relative error of <5% in sensitivity of the method) were calculated therefore the developed dual-emission ratiometric fluorescent nanosensor is able to detect MTF with a good selectivity in real samples.[51,52]

3.9. Application of the developed method for the determination of MTF in plasma samples

To study the practical applicability of the designed ratiometric method, the method was applied to measure MTF in spiked plasma samples (Table 5). Validation experiments were also done by spiking certain concentrations of the MTF standard into real samples, before any preparation process. Finally, MTF concentrations were quantified following the general procedure described in the experimental section. The results are shown in Table 5, which indicates suitable recoveries.

Table 3 Details of the stability of the proposed method in plasma samples

Sample	Con. (M)	Short-time temperature (detected)	Recovery (%)	Freeze-thaw (detected)	Recovery (%)
Plasma	3.0×10^{-8}	2.6×10^{-8}	87.3	2.7×10^{-8}	92.7
	5.0×10^{-8}	4.5×10^{-8}	91.7	4.1×10^{-8}	82.7
	3.0×10^{-6}	2.8×10^{-8}	96.4	2.9×10^{-6}	99.4
	5.0×10^{-6}	5.2×10^{-8}	105.4	5.0×10^{-6}	101.1

Table 5 Determination of MTF in spiked plasma samples

Sample	Added (M)	Found (M)	Recovery (%)
Plasma	3.0×10^{-9}	3.5×10^{-9}	118.8
	7.0×10^{-9}	7.8×10^{-9}	111.5
	5.0×10^{-8}	5.0×10^{-8}	100.3
	5.0×10^{-7}	4.6×10^{-7}	93.9
	5.0×10^{-6}	5.0×10^{-6}	100.1
	9.0×10^{-6}	9.4×10^{-6}	104.8

4. Conclusion

In conclusion, in the present study, N-GQDs/Tb–Phen NPs was synthesized and characterized by using different methods. It was observed that the synthesized nanosystem showes two characteristic emission band, which was used as a rapid, highly sensitive, and selective ratiometric fluorescent nanosensor for the detection of MTF in a test tube and biological samples. Optimization of the experimental conditions was performed and the results confirmed that the maximum fluorescence intensity ratio was observed under the conditions of 0.05 M acetate buffer solution with pH 7.5 and 20 °C. Also, detection of MTF was carried out using the plasma and spiked human serum sample with a wide linear range of 1.0 nM to 7.0 μM respectively, and LOD values were also calculated to be 0.76 nM. So, this nanosensor is highly promising to be useful for detecting MTF in biological samples with high sensitivity and selectivity.

Conflicts of interest

We have no conflict of interest to declare.

Acknowledgements

References

1 M. Mirzaei, M. Rahmaninan, M. Mirzaei and A. Nadjarzadeh, Epidemiology of diabetes mellitus, pre-diabetes, undiagnosed and uncontrolled diabetes in Central Iran: results from Yazd health study, *BMC Public Health*, 2020, **20**(1), 1–9.

2 S. B. Aynalem and A. J. Zeleke, Prevalence of diabetes mellitus and its risk factors among individuals aged 15 years and above in Mizan-Aman town, Southwest Ethiopia, 2016: a cross sectional study, *Int. J. Endocrinol.*, 2018, **2018**, 9317987.

3 A. B. Olokoba, O. A. Obateru and L. B. Olokoba, Type 2 diabetes mellitus: A review of current trends, *Oman Med. J.*, 2012, **27**(4), 269.

4 D. R. El-Wasseef, Simultaneous determination of metformin, nateglinide and gliclazide in pharmaceutical preparations using micellar liquid chromatography, *Int. J. Biomed. Sci.*, 2012, **8**(2), 144.

5 S. Azarian, M. Shaghaghi, G. Dehghan and N. Sheibani, A rapid, simple and ultrasensitive spectrofluorimetric method for the direct detection of metformin in real samples based on a nanoquenching approach, *Luminescence*, 2021, **36**(3), 658–667.

6 K. Chaudhari, J. Wang, Y. Xu, A. Winters, L. Wang, X. Dong, E. Y. Cheng, R. Liu and S.-H. Yang, Determination of metformin bio-distribution by LC-MS/MS in mice treated with a clinically relevant paradigm, *PLoS One*, 2020, **15**(6), e0234571.

7 M. Shaghaghi, G. Dehghan, S. Rashtbari, N. Sheibani and A. Aghamohammadi, Multispectral and computational probing of the interactions between sitagliptin and serum albumin, *Spectrochim. Acta, Part A*, 2019, **223**, 117286.

8 K. H. Yuen and K. K. Peh, Simple high-performance liquid chromatographic method for the determination of metformin in human plasma, *J. Chromatogr. B: Biomed. Sci. Appl.*, 1998, **710**(1–2), 243–246.

9 R. Vetapalem, R. P. Yejella and L. R. Atmakuri, Development and validation of a stability indicating RP-HPLC method for simultaneous estimation of teneligliptin and metformin, *Turk. J. Pharm. Sci.*, 2020, **17**(2), 141.

10 D. Mohamed, M. S. Elshahed, T. Nasr, N. Aboutaleb and O. Zakaria, Novel LC–MS/MS method for analysis of metformin and canagliflozin in human plasma: application to a pharmacokinetic study, *BMC Chem.*, 2019, **13**(1), 1–11.

11 D. Patel, P. Kumar, S. Sharma and J. Dwivedi, Analytical methods for metformin estimation, *Crit. Rev. Anal. Chem.*, 2017, **47**(5), 405–417.

12 S. Rashtbari, G. Dehghan, S. Khataee, M. Amini and A. Khataee, Dual enzymes-mimic activity of nanolayered manganese-calcium oxide for fluorometric determination of metformin, *Chemosphere*, 2021, 133063.

13 R. Ali, F. M. Alminderej and S. M. Saleh, A simple, quantitative method for spectroscopic detection of metformin using gold nanoclusters, *Spectrochim. Acta, Part A*, 2020, **241**, 118744.

14 E. Uçaktürk, The development and validation of a gas chromatography-mass spectrometry method for the determination of metformin in human plasma, *Anal. Methods*, 2013, **5**(18), 4723–4730.

15 M. Salim, N. El-Enany, F. Belal, M. Walash and G. Patonay, Simultaneous determination of sitagliptin and metformin in pharmaceutical preparations by capillary zone electrophoresis and its application to human plasma analysis, *Anal. Chem. Insights*, 2012, **7**, S9940.

16 H. P. Chhetri, P. Thapa and A. Van Schepdael, Simple HPLC-UV method for the quantification of metformin in human plasma with one step protein precipitation, *Saudi Pharm. J.*, 2014, **22**(5), 483–487.

17 P. Vemula, D. Dodda, U. Balekari, S. Panga and C. Veeresham, Simultaneous determination of linagliptin

and metformin by reverse phase-high performance liquid chromatography method: An application in quantitative analysis of pharmaceutical dosage forms, *J. Adv. Pharm. Technol. Res.*, 2015, **6**(1), 25.

18 F. A. Siddiqui, N. Sher, N. Shafi and S. S. Bahadur, Concurrent determination of Metformin and some ACE inhibitors: its application to pharmacokinetics, *Arabian J. Chem.*, 2017, **10**, S2979–S2987.

19 A. Liu and S. P. Coleman, Determination of metformin in human plasma using hydrophilic interaction liquid chromatography–tandem mass spectrometry, *J. Chromatogr. B: Anal. Technol. Biomed. Life Sci.*, 2009, **877**(29), 3695–3700.

20 J. Soleymani, M. Hasanzadeh, M. H. Somi, S. A. Ozkan and A. Jouyban, Targeting and sensing of some cancer cells using folate bioreceptor functionalized nitrogen-doped graphene quantum dots, *Int. J. Biol. Macromol.*, 2018, **118**, 1021–1034.

21 K. P. Gopinath, D.-V. N. Vo, D. G. Prakash, A. A. Joseph, S. Viswanathan and J. Arun, Environmental applications of carbon-based materials: A review, Environ, *Chem. Lett.*, 2021, **19**(1), 557–582.

22 J. Jiménez-López, E. Llorent-Martínez, P. Ortega-Barrales and A. Ruiz-Medina, Graphene quantum dots-silver nanoparticles as a novel sensitive and selective luminescence probe for the detection of glyphosate in food samples, *Talanta*, 2020, **207**, 120344.

23 G. Ge, L. Li, D. Wang, M. Chen, Z. Zeng, W. Xiong, X. Wu and C. Guo, Carbon dots: Synthesis, properties and biomedical applications, *J. Mater. Chem. B*, 2021, **9**, 6553–6575.

24 A. Kalluri, D. Debnath, B. Dharmadhikari and P. Patra, Graphene quantum dots: Synthesis and applications, *Methods Enzymol.*, 2018, **609**, 335–354.

25 D. Ghosh, K. Sarkar, P. Devi, K.-H. Kim and P. Kumar, Current and future perspectives of carbon and graphene quantum dots: From synthesis to strategy for building optoelectronic and energy devices, *Renewable Sustainable Energy Rev.*, 2021, **135**, 110391.

26 Z. Farka, T. Jurik, D. Kovář, L. Trnkova and P. Skládal, Nanoparticle-based immunochemical biosensors and assays: Recent advances and challenges, *Chem. Rev.*, 2017, **117**(15), 9973–10042.

27 M. Nurunnabi, Z. Khatun, K. M. Huh, S. Y. Park, D. Y. Lee, K. J. Cho and Y.-k. Lee, In vivo biodistribution and toxicology of carboxylated graphene quantum dots, *ACS Nano*, 2013, 7(8), 6858–6867.

28 H. Wang, P. Agarwal, S. Zhao, J. Yu, X. Lu and X. He, A biomimetic hybrid nanoplatform for encapsulation and precisely controlled delivery of theranostic agents, *Nat. Commun.*, 2015, **6**(1), 1–13.

29 X. T. Zheng, A. Than, A. Ananthanaraya, D.-H. Kim and P. Chen, Graphene quantum dots as universal fluorophores and their use in revealing regulated trafficking of insulin receptors in adipocytes, *ACS Nano*, 2013, 7(7), 6278–6286.

30 I. Al-Ogaidi, H. Gou, Z. P. Alar, S. Guo, A. K. Melconian, A. K. A. Al-Kazaz, F. Meng and N. Wu, Detection of the ovarian cancer biomarker CA-125 using chemiluminescence resonance energy transfer to graphene quantum dots, *Chem. Commun.*, 2014, **50**(11), 1344–1346.

31 A. Kolay, R. K. Kokal, A. Kalluri, I. Macwan, P. K. Patra, P. Ghosal and M. Deepa, New antimony selenide/nickel oxide photocathode boosts the efficiency of graphene quantum-dot co-sensitized solar cells, *ACS Appl. Mater. Interfaces*, 2017, **9**(40), 34915–34926.

32 R. Li, X. Wang, Z. Li, H. Zhu and J. Liu, Folic acid-functionalized graphene quantum dots with tunable fluorescence emission for cancer cell imaging and optical detection of Hg 2+, *New J. Chem.*, 2018, **42**(6), 4352–4360.

33 M. H. Lee, J. S. Kim and J. L. Sessler, Small molecule-based ratiometric fluorescence probes for cations, anions, and biomolecules, *Chem. Soc. Rev.*, 2015, **44**(13), 4185.

34 G. Dehghan, M. Shaghaghi and P. Alizadeh, A novel ultrasensitive and non-enzymatic "turn-on-off" fluorescence nanosensor for direct determination of glucose in the serum: As an alternative approach to the other optical and electrochemical methods, *Spectrochim. Acta, Part A*, 2019, **214**, 459–468.

35 M. Shaghaghi, S. Rashtbari, A. Abdollahi, G. Dehghan and A. Jouyban, A Sensitive, simple and Direct Determination of Pantoprazole Based on a "Turn off-on" Fluorescence Nanosensor by Using Terbium-1, 10-phenanthroline-silver Nanoparticles, *Anal. Sci.*, 2020, **36**(11), 1345–1352.

36 J. Liu, Y. Li, L. Liu, Y. Gao, Y. Zhang, Z. Yin, F. Pi and X. Sun, Current Progress on Antibiotic Sensing Based on Ratiometric Fluorescent Sensors, *Bull. Environ. Contam. Toxicol.*, 2021, **107**(2), 176–184.

37 H. Safardoust-Hojaghan and M. Salavati-Niasari, Degradation of methylene blue as a pollutant with N-doped graphene quantum dot/titanium dioxide nanocomposite, *J. Cleaner Prod.*, 2017, **148**, 31–36.

38 Z. Qi and Y. Chen, Charge-transfer-based terbium MOF nanoparticles as fluorescent pH sensor for extreme acidity, *Biosens. Bioelectron.*, 2017, **87**, 236–241.

39 H. Tan, B. Liu and Y. Chen, Lanthanide coordination polymer nanoparticles for sensing of mercury (II) by photoinduced electron transfer, *ACS Nano*, 2012, **6**(12), 10505–10511.

40 S. Rashtbari, G. Dehghan and M. Amini, An ultrasensitive label-free colorimetric biosensor for the detection of glucose based on glucose oxidase-like activity of nanolayered manganese-calcium oxide, *Anal. Chim. Acta*, 2020, **1110**, 98–108.

41 D. Wang, J. Zhang, Q. Lin, L. Fu, H. Zhang and B. Yang, Lanthanide complex/polymer composite optical resin with intense narrow band emission, high transparency and good mechanical performance, *J. Mater. Chem.*, 2003, **13**(9), 2279–2284.

42 J. Zhang, L.-X. Wang, L. Zhang, Y. Chen and Q.-T. Zhang, Co-luminescence properties of terbium ions–benzoic acid–phen complexes doped with europium ions, *Rare Metals*, 2013, **32**(6), 599–604.

43 N.-V. Cuong, Y.-L. Li and M.-F. Hsieh, Targeted delivery of doxorubicin to human breast cancers by folate-decorated

star-shaped PEG–PCL micelle, *J. Mater. Chem.*, 2012, **22**(3), 1006–1020.

44 Z. Qi, Q. You and Y. Chen, Nucleotide/Tb3+ coordination polymer nanoparticles as luminescent sensor and scavenger for nitrite ion, *Anal. Chim. Acta*, 2016, **902**, 168–173.

45 A. Halmemies-Beauchet-Filleau, A. Vanhatalo, V. Toivonen, T. Heikkilä, M. Lee and K. Shingfield, Effect of replacing grass silage with red clover silage on nutrient digestion, nitrogen metabolism, and milk fat composition in lactating cows fed diets containing a 60: 40 forage-to-concentrate ratio, *J. Dairy Sci.*, 2014, **97**(6), 3761–3776.

46 A. Hasanzadeh, F. Radmanesh, J. Kiani, M. Bayandori, Y. Fatahi, A. R. Aref and M. Karimi, Photoluminescent functionalized carbon dots for CRISPR delivery: Synthesis, optimization and cellular investigation, *Nanotech*, 2019, **30**(13), 135101.

47 J. L. Manzoori, A. Jouyban, M. Amjadi and J. Soleymani, Spectrofluorimetric determination of folic acid in tablets and urine samples using 1, 10-phenanthroline-terbium probe, *Luminescence*, 2011, **26**(2), 106–111.

48 M. O. Pujol, D. J. Coleman, C. D. Allen, O. Heidenreich and D. A. Fulton, Determination of key structure–activity relationships in siRNA delivery with a mixed micelle system, *J Con. Rel*, 2013, **172**(3), 939–945.

49 M. Gazizadeh, G. Dehghan and M. Amjadi, Ultrasensitive detection of glibenclamide based on its enhancing effect on the fluorescence emission of CdTe quantum dots, *Luminescence*, 2019, **34**(2), 297–303.

50 Food and Drug Administration, *Guidance for Industry: Bioanalytical Method Validation*, 2001, accessed 10 Sept 2013, 2017, **https://www.fda.gov/downloads/Drugs.Guidances/ucm070107.pdf**.

51 M. Ghaedi, A. Shokrollahi, F. Ekrampour and R. Aghaei, Sensitized spectrophotometric determination of trace amounts of copper (II) ion using diacetyl monooxime in surfactant media, *Bull Chem Soc Ethiop*, 2009, **23**(3).

52 R. Shokri and M. Amjadi, A ratiometric fluorescence sensor for triticonazole based on the encapsulated boron-doped and phosphorous-doped carbon dots in the metal organic framework, *Spectrochim. Acta, Part A*, 2021, **246**, 118951.

53 J. Narang, N. Malhotra, C. Singhal, R. Bhatia, V. Kathuria and M. Jain, Graphene nanoflakes on transparent glass electrode sensor for electrochemical sensing of anti-diabetic drug, *Bioprocess Biosyst. Eng.*, 2017, **40**(4), 537–548.

54 S. Momeni, M. Farrokhnia, S. Karimi and I. Nabipour, Copper hydroxide nanostructure-modified carbon ionic liquid electrode as an efficient voltammetric sensor for detection of metformin: a theoretical and experimental study, *J. Iran. Chem. Soc.*, 2016, **13**(6), 1027–1035.